Advances in Nano Research, *Vol. 9, No. 3 (2020) 157-172*
DOI: https://doi.org/10.12989/anr.2020.9.3.157

Size dependent axial free and forced vibration of carbon nanotube via different rod models

Farshad Khosravi[1a], Mahdi Simyari[2b], Seyed A. Hosseini[*3] and Abdelouahed Tounsi[4c]

[1]*Department of Aerospace Engineering, K.N. Toosi University of Technology, Tehran, Iran*
[2]*Department of Mechanical Engineering, University of Tehran, Tehran, Iran*
[3]*Department of Industrial, Mechanical and Aerospace Engineering, Buein Zahra Technical University, Buein Zahra, Qazvin, Iran*
[4]*Yonsei Frontier Lab, Yonsei University, Seoul, Korea*

(*Received September 6, 2019, Revised August 11, 2020, Accepted August 13, 2020*)

Abstract. The aim of this present research is the effect of the higher-order terms of the governing equation on the forced longitudinal vibration of a nanorod model and making comparisons of the results with classical nonlocal elasticity theory. For this purpose, the free axial vibration along with forced one under the two various linear and harmonic axial concentrated forces in zigzag Single-Walled Carbon Nanotube (SWCNT) are analyzed dynamically. Three various theories containing the classical theory, which is called Eringen's nonlocal elasticity, along with Rayleigh and Bishop theories (higher-order theories) are established to justify the nonlocal behavior of constitutive relations. The governing equation and the related boundary conditions are derived from Hamilton's principle. The assumed modes method is adopted to solve the equation of motion. For the free axial vibration, the natural frequencies are calculated for the various values of the nonlocal parameter only based on Eringen's theory. The effects of the nonlocal parameter, thickness, length, and ratio of the excitation frequency to the natural frequency over time in dimensional and non-dimensional axial displacements are investigated for the first time.

Keywords: forced vibration; Bishop theory; Rayleigh theory; carbon nanotube; axial vibration; assumed modes method

1. Introduction

Nanotechnology is established based on the manipulation of the atoms and molecules in nanoscale to produce the nanostructures (Adams and Barbante 2013). It was introduced by Richard P. Feynman about 60 years ago. Since then, it has been utilized in the different aspects of science, including textile (Joshi *et al*. 2008), water cleaning (Diallo *et al*. 2009), transistors (Chau *et al*. 2005), medicine (Caruthers *et al*. 2007), etc. As a nanostructure, nanotubes possess the strongest and most resilient materials in nature (Dai 2002). Also, they have a hexagonal shape, and this property has made them have a delicate structure.

Carbon Nanotubes (CNTs) are seamless layers of rolled-up graphene, which depending on their applications, are divided into two different types, including single-walled and multi-walled. The invention of carbon nanotube occurred by Iijima (Iijima 1991, Harris and Harris 2009). Afterward, it captured the attention towards themselves since now (Bethune *et al*. 1993). Most part of the fabrication of the CNTs is dedicated to bulk composite materials and thin films (De Volder *et al*. 2013). CNTs can be separated into smaller pieces (Ajayan 1999), and their applications can be contained different fields, including biomedicine (Bianco *et al*. 2005, Sinha and Yeow 2005), bioelectronics (Miyako *et al*. 2011, Iost and Crespilho 2012), sensors (Sherigara *et al*. 2003, Suehiro *et al*. 2003, Gooding 2005), industrial application (Yumura 2003, Makar and Beaudoin 2004, Paradise and Goswami 2007), pharmacy, medicine (He *et al*. 2013), etc. Single-Walled Carbon Nanotubes (SWCNTs) have vast applications such as extremely high values of Young's modulus (Kelly 1981), high electrical (Thess *et al*. 1996), thermal conductivity (Glory *et al*. 2008). Also, they are light and flexible (Esawi and Farag 2007).

The nonlocal elasticity theory, which was first introduced by Eringen (1983), has been chosen to show the nonlocality, while there are some other studies done by this theory, as well as nonlocal strain gradient theory, modified couple stress theory and surface effects as references (Mehralian and Beni 2017, Zeighampour *et al*. 2017a, b, Bastanfar *et al*. 2019, Hosseini *et al*. 2019, Alizadeh Hamidi *et al*. 2020, Hamidi *et al*. 2020, Hosseini and Khosravi 2020, Hosseini *et al*. 2020, Khosravi and Hosseini 2020, Khosravi *et al*. 2020a, b, c, d, e, f). Mehar and Panda (2019) utilized higher-order mid-plane kinematics and multiscale models considering two different in-plane thermal loadings to investigate the buckling raised from the thermal environment in nanocomposites curved shell structures. Akbaş (2018) investigated the forced vibration of the FG microbeams containing crack, considering the damping effects in the time domain based on the Kelvin-Voigt model and modified couple stress theory. Bensaid *et al*. (2018) carried out the free vibration analysis of nanobeam

*Corresponding author, Assistant Professor,
E-mail: hosseini@bzte.ac.ir
[a] Student, E-mail: fkhosravi@mail.kntu.ac.ir
[b] Student, E-mail: msimyari@ut.ac.ir
[c] Professor, E-mail: tou_abdel@yahoo.com

ISSN: 2287-237X (Print), 2287-2388 (Online)

embedded in an elastic foundation considering the shear deformation effect based on the nonlocal strain gradient theory and higher-order hyperbolic beam model. Ebrahimi *et al*. (2019) investigated the wave propagation in the magneto-electro-elastic nanotubes based on the nonlocal elasticity theory along with the shell model. The phase velocity, as well as the wave frequency, were measured in their research. Boutaleb *et al*. (2019) worked on the dynamic vibrational behavior of the rectangular FG nanoplates using the nonlocal elasticity theory as well as the quasi 3D high shear deformation theory.

Wang and Liew (2007) investigated the effect of the static deformation of the nano-dimension materials based on the nonlocal Euler-Bernoulli and Timoshenko beam theory. Şimşek (2011) studied on the double-carbon nanotube systems connected with elastic spring affected by a moving nanoparticle in one of the nanotubes. The influence of the nonlocal parameter, aspect ratio, velocity and elastic effect demonstrated dynamically. A giga-hertz oscillator examined in a uniform, concentric of CNTs by Cox *et al*. (2008). Aydogdu and Filiz (2011) used Eringen's nonlocal elasticity theory to investigate the free axial response for different boundary conditions and lengths of the CNT when a mass attached to it. Eltaher *et al*. (2013) analyzed the vibration of a Euler-Bernoulli nanobeam based on Eringen's theory to represent the nonlocality and solved the constitutive relations by a finite element method. Georgantzinos and Anifantis (2010) used SWCNT and MWCNT mass resonant sensor with an attached mass on them. Also, the fundamental frequencies with respect to the position of the attached nanoparticle and mass were measured. Shen and Zhu (2012) studied the post-buckling due to the temperature rising in a homogenous sandwich plate surrounded by CNTs as reinforced-composite on the elastic foundation. Shenas *et al*. (2017) paid to the FG-CNTRC pre-twisted nanobeams affected by the thermal parameter. The influence of the fluid flow in the axial vibration of SWCNT and also the stability of it analyzed by Oveissi *et al*. (2016). Rahmani *et al*. (2017) simulated a thermal load in curved microbeam and analyzed the buckling and free response of the system based on the strain gradient theory. Lei *et al*. (2013) utilized the FG-CNT as a reinforced composite panel in the axial direction and established an element-free kp-Ritz method to calculate the free vibrations. Liu *et al*. (2009) worked on the vibration of the nanobeam subjected to both distributed axial and torsional loadings simultaneously. Aydogdu (2009) showed the small-scale effect on the axial vibration of the nanorod for different boundary conditions. Mohammadian *et al*. (2019) presented a new nonlocal model for the hetero-junction nanorods and investigated the effect of the conjunction point, attached mass and some other parameters on the free axial vibration. Danesh *et al*. (2012) established the nonlocal elasticity theory to analyze the axial vibration of the tapered nanorod under the different boundary conditions and showed the nonlocal effect in reduction of the frequencies. Wang *et al*. (2009) investigated the surface effects and size-dependency on the axial buckling and transverse vibration in a nanowire, based on the refined Timoshenko beam theory. Aydogdu (2015) studied the effect of the van der Waals, geometrical effect and the small-scale parameter in axial vibration of the DWCNT. Li *et al*. (2010) investigated a nanobeam under the axial tensional and compressive forces and the natural frequencies raised from transverse vibrations dynamically, also the effects of the nonlocal parameter, axial forces and the stability of it have been discussed in their study. The effect of the nonlocality in the amplitude of the forced vibration of a CNT based on Euler-Bernoulli theory for two local and nonlocal theories was examined by Karaoglu and Aydogdu (2010). They concluded that the amplitude based on the nonlocal theory is greater in comparison with the local one. Natsuki *et al*. (2014) worked on the CNT under the tensional loading with clamped boundary condition and attached mass to obtain the resonant frequencies and frequency shifts using Euler–Bernoulli beam theory and Rayleigh's energy method.

Kunche *et al*. (2019) carried out the modal frequencies of adhesive bonded T-joint structures with theoretical and experimental methods. There are different studies in which conduct the buckling, deflection, flexural or other mechanical behavior of the curved sandwiches and laminated composites numerically under various environments (Panda and Katariya 2015, Katariya *et al*. 2017, 2018, Mehar *et al*. 2017a, b, 2018a, b, c, Mehar and Panda 2018a, 2020, Katariya and Panda 2019a, b, c, Pandey *et al*. 2019).

The eigenfrequency of the nanoplates via finite element method and higher-order model (Mehar *et al*. 2018a), the nonlinear responses of the curved FG sandwich based on the finite element method (Mehar *et al*. 2018b) and the flexural behavior of the functionally graded carbon nanotube-reinforced doubly curved shell panel by mathematical model have been developed (Mehar and Panda 2018b) and the frequency of the multi-walled carbon nanotube-reinforced polymer composite was computed using generic higher-order shear deformation kinematics (Mehar *et al*. 2017a). In neither of the aforementioned studies, the dynamic forced axial displacement through nonlocal Bishop, Rayleigh, and Eringen elasticity theories for different loadings and boundary conditions have not been conducted. Such theories, namely Rayleigh and Bishop theories are taking into account the effects of inertia of the lateral motion and the shear stiffness. Thus, it leads the study to become a novel and more accurate. In this context, the axial displacement under the concentrated force in zigzag SWCNT is studied. The concentrated forces include linear and harmonic loads. The Eringen's nonlocal elasticity theory (classical theory), as well as Rayleigh and Bishop theories, are utilized to demonstrate the nonlocality.

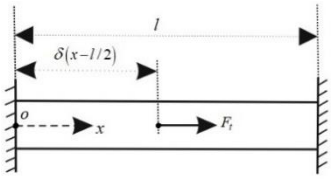

Fig. 1 Zigzag SWCNT subjected to a concentrated force for clamped-clamped (C-C) boundary condition

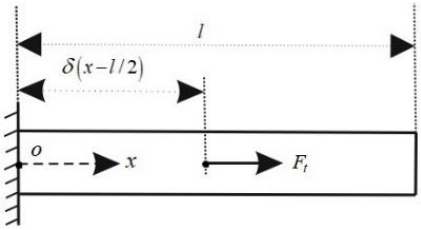

Fig. 2 Zigzag SWCNT subjected to a concentrated force for clamped-free (C-F) boundary condition

The assumed modes method is used to derive the governing equation and boundary conditions. The effect of the nonlocal parameter is investigated for calculating the natural frequencies. Moreover, the influences of the nonlocal parameters, thickness, length and excitation frequency in the time domain are described in the forced analysis.

2. Nonlocal SWCNT model

A SWCNT under the axial concentrated loading subjected to the middle of the body has been indicated in Figs. 1 and 2 where l and f_0 represent the length and the axial concentrated force in the direction of the x-axis, y and z axes are in the direction of the CNT's radius.

Fig. 1 demonstrates the SWCNT with a zigzag structure under the concentrated force with the clamped-clamped boundary condition, while Fig. 2 represents the SWCNT under the clamped-free boundary condition. In this study, this force is linear and harmonic for both states. The displacement fields for the CNT due to the axial force can be expressed as

$$\begin{aligned} u &= u(x,t) \\ v &= 0 \\ w &= 0 \end{aligned} \tag{1}$$

where u denotes the axial displacement and v and w are the transverse displacements toward the y and z axes, respectively. All the displacements occur at any arbitrary point $(x,\ 0)$. The non-zero strain displacements due to the axial displacement can be stated as

$$\begin{aligned} &\varepsilon_{xx} = \frac{\partial u}{\partial x}, \qquad \varepsilon_{xy} = \varepsilon_{xz} = \varepsilon_{yz} = 0 \\ &\varepsilon_{yy} = \varepsilon_{zz} = 0 \end{aligned} \tag{2}$$

where ε_{xx} represents the axial strain.

2.1 Hamilton's principle

Hamilton's principle in the time interval of $t_1 < t < t_2$ for deriving the governing equation and associated boundary condition can be expressed as follows

$$\int_0^t \delta(\Pi - T - W)dt = 0 \tag{3}$$

where Π, T and W represent the potential energy, kinetic energy and external work, respectively. The first variation of the potential energy can be written as

$$\delta U = \int_V \sigma_{xx}\delta\varepsilon_{xx}dV \tag{4}$$

Substituting the non-zero term of Eq. (2) in Eq. (4) leads to

$$\delta U = \int_V \left(\sigma_{xx}\left(\frac{\partial \delta u}{\partial x}\right)\right)dV = \int_0^l N\left(\frac{\partial \delta u}{\partial x}\right)dx \tag{5}$$

where N is the axial force and equals to

$$N = \int_A \sigma_{xx}dA \tag{6}$$

The first variation of the kinetic energy from Hamilton's principle can be stated as

$$\delta T_K = \frac{1}{2}\rho A\int_0^l \delta\left(\frac{\partial u}{\partial t}\right)^2 dx = \rho A\int_0^l \left(\frac{\partial u}{\partial t}\frac{\partial \delta u}{\partial t}\right)dx \tag{7}$$

The first variation of the external work due to the concentrated force is given by

$$\delta W = \int_0^l f(x,t)\delta u dx \tag{8}$$

The resultant of the substitution of Eqs. (5), (7) and (8) into Eq. (3) is brought as follows

$$\int_0^t \left(N\delta u\Big|_0^l - \int_0^l \frac{\partial N}{\partial x}\delta u dx + \rho A\int_0^l \frac{\partial^2 u}{\partial t^2}\delta u dx - \int_0^l f(x,t)\delta u dx\right) \tag{9}$$

From above, the governing equation can be stated as

$$\frac{\partial N}{\partial x} = \rho A\frac{\partial^2 u}{\partial t^2} - f(x,t) \tag{10}$$

Subsequently, the associated boundary condition is given by

$$N\Big|_0^l = 0 or \delta u\Big|_0^l = 0 \tag{11}$$

The nonlocal constitutive relations for a CNT according to the Eringen's nonlocal elasticity theory can be expressed as

$$\sigma^{nl} - \mu\frac{\partial^2 \sigma^{nl}}{\partial x^2} = E\varepsilon^{nl} \tag{12}$$

Here σ^{nl}, ε^{nl}, μ and E denote the nonlocal stress, strain, nonlocal parameter and Young's modulus, respectively. The nonlocal parameter also can be rewritten as $\mu = (e_0 a)^2$. For the CNT under the axial force, the constitutive equation in Eq. (12) can be rewritten as

$$\sigma_{xx} - \mu \frac{\partial^2 \sigma_{xx}}{\partial x^2} = E\varepsilon_{xz} \tag{13}$$

Integrating Eq. (13) with respect to the cross-sectional area leads to

$$N - \mu \frac{\partial^2 N}{\partial x^2} = EA\varepsilon_{xx} \tag{14}$$

By substitution of the first derivate of Eq. (10) into Eq. (14), we will have

$$N = \mu \left(\rho A \frac{\partial^3 u}{\partial x \partial t^2} - \frac{\partial f(x,t)}{\partial x} \right) + EA \frac{\partial u}{\partial x} \tag{15}$$

Consequently, by replacing the first derivative of Eq. (15) into Eq. (10), the finalized governing equation of motion for SWCNT can be expressed as

$$f(x,t) - \rho A \frac{\partial^2 u}{\partial t^2} + \mu \left(\rho A \frac{\partial^4 u}{\partial x^2 \partial t^2} - \frac{\partial^2 f(x,t)}{\partial x^2} \right) + EA \frac{\partial^2 u}{\partial x^2} = 0 \tag{16}$$

3. Analytical solution

3.1 Free axial vibration

Free-axial vibration occurs when all the axial forces set to be zero. By doing so, Eq. (6) changes to the following format

$$\rho A \frac{\partial^2 u}{\partial t^2} - \mu \left(\rho A \frac{\partial^4 u}{\partial x^2 \partial t^2} \right) - EA \frac{\partial^2 u}{\partial x^2} = 0 \tag{17}$$

In order to solve Eq. (17), the axial displacement should be discretized in two time-dependent and position-dependent parts as

$$u(x,t) = \sum_{n=1}^{\infty} U_n(x) e^{i\omega t} \tag{18}$$

By applying Eq. (18) into Eq. (17), the governing equation can be rewritten as

$$\rho A \omega^2 U_n + EAU_n'' - \mu(\rho A \omega^2 U_n'') = 0 \tag{19}$$

in which U_n and U_n'' in Eq. (19) represent the nth mode shape and the second derivative of it, respectively, and are equivalent to

$$U_n(x) = C_n \sin(Px) \tag{20}$$

$$U_n''(x) = -C_n P^2 \sin(Px) \tag{21}$$

Furthermore, the value of P for clamped-clamped and clamped-free boundary conditions is equivalent to the following statements, respectively

$$P = \frac{n\pi}{l} \tag{22}$$

$$P = \frac{(2n-1)\pi}{2l} \tag{23}$$

The natural frequency can be calculated by substituting Eqs. (22) and (23) into Eq. (19) as follows

$$\rho A \omega^2 - EAP^2 + \mu P^2 (\rho A \omega^2) = 0 \tag{24}$$

Solving Eq. (24) leads to calculate the dimensional and non-dimensional natural frequencies for both clamped-clamped and clamped-free boundary conditions. This value for the clamped-clamped boundary condition can be stated as

$$\omega_n = \sqrt{\frac{E\left(\frac{n\pi}{l}\right)^2}{\rho\left(1 + \mu\left(\frac{n\pi}{l}\right)^2\right)}} \tag{25}$$

$$\bar{\omega}_n = \sqrt{\frac{(n\pi)^2}{\left(1 + \mu\left(\frac{n\pi}{l}\right)^2\right)}} \tag{26}$$

where ω_n and $\bar{\omega}_n$ are the dimensional and non-dimensional natural frequencies for the clamped-clamped CNT, respectively.

Subsequently, for the clamped-free CNT, it can be expressed as

$$\omega_n = \sqrt{\frac{E\left(\frac{(2n-1)\pi}{2l}\right)^2}{\rho\left(1 + \mu\left(\frac{(2n-1)\pi}{2l}\right)^2\right)}} \tag{27}$$

$$\bar{\omega}_n = \frac{1}{2}\sqrt{\frac{\left((2n-1)\pi\right)^2}{\left(1 + \mu\left(\frac{(2n-1)\pi}{2l}\right)^2\right)}} \tag{28}$$

Here ω_n and $\bar{\omega}_n$ represent the dimensional and non-dimensional natural frequencies for the clamped-free CNT, respectively.

3.2 Forced axial vibration

To analyze the axial displacement dynamically, the discretized axial displacement can be stated as

$$u(x,t) = \sum_{n=1}^{\infty} U_n(x)\eta_n(t) \tag{29}$$

where $\eta_n(t)$ represents the unknown time-dependent generalized coordinates. Using Eq. (29) in Eq. (16) leads to

$$f(x,t) - \sum_{n=1}^{\infty} (\rho A) U_n(x) \ddot{\eta}_n(t) - \mu \left(\sum_{n=1}^{\infty} (\rho A) P^2 U_n(x) \ddot{\eta}_n(t) + \frac{\partial^2 f(x,t)}{\partial x^2} \right) - EAP^2 \sum_{n=1}^{\infty} U_n(x)\eta_n(t) = 0 \tag{30}$$

In order to normalize and modal solving Eq. (30) should be multiplied by $U_m(x)$ as follows

$$\int_0^l [f(x,t)-\mu(f''(x,t))]U_m(x)dx-\ddot{\eta}_n(t)(\rho A(1+\mu P^2)\int_0^l U_n(x)U_m(x)dx\Big)-\eta_n(t)\left(EAP^2\int_0^l U_n(x)U_m(x)dx\right)=0 \quad (31)$$

in which, the orthogonally relation for normal mode of CNT can be stated as

$$\int_0^l U_n(x)U_m(x)dx=\begin{cases}1 & m=n\\ 0 & m\neq n\end{cases} \quad (32)$$

Replacing Eq. (20) into Eq. (32) results in

$$C_n^2\int_0^l sin^2(Px)dx=1 \quad (33)$$

where the coefficient C_n for nth mode is equal to

$$C_n=\sqrt{\frac{2}{l}}n=1,2,... \quad (34)$$

The mode shape and the second derivative of the mode shape of Eqs. (20) and (21) for the obtained values in Eq. (34) changes into the following statements

$$U_n(x)=\sqrt{\frac{2}{l}}sin(Px) \quad (35)$$

$$U_n''(x)=-\sqrt{\frac{2}{l}}P^2\,sin(Px) \quad (36)$$

Considering Eq. (32), Eq. (31) can be simplified as

$$\rho A(1+\mu(P)^2)\ddot{\eta}_n(t)+EA(P)^2\eta_n(t)=\int_0^l[f(x,t)-\mu(f''(x,t))]U_m(x)dx \quad (37)$$

Eq. (37) can be rewritten as follows

$$\ddot{\eta}_n(t)+{\lambda_n}^2\eta_n(t)=\zeta_n F_n(t) \quad (38)$$

where

$$\lambda_n=\frac{E(P)^2}{\sqrt{\rho(1+\mu(P)^2)}} \quad (39)$$

$$\zeta_n=\frac{1}{\rho A(1+\mu(P)^2)} \quad (40)$$

The time-dependent axial concentrated force $F_n(t)$ in nth mode can be expressed as

$$F_n(t)=\zeta_n\int_0^l[f(x,t)-\mu(f''(x,t))]U_m(x)dx \quad (41)$$

The steady state for obtaining the time-dependent generalized coordinates disregarding the initial conditions can be stated as

$$\eta_n(t)=\frac{1}{\lambda_n}\int_0^t F_n(\tau)\,sin\,\lambda_n\,(t-\tau)d\tau \quad (42)$$

3.2.1 Linear axial concentrated force

Since the concentrated force subjected to the middle of the CNT (i.e., $x=l/2$), $f(x,t)$ can be defined as

$$f(x,t)=F_n(t)\delta\left(x-\frac{l}{2}\right)=f_0 t\,\delta\left(x-\frac{l}{2}\right) \quad (43)$$

where $F_n(t)$ is the linear time-dependent load, f_0 represents the amplitude of the load, and is linear. Using Eq. (45) and the second derivative of it in Eq. (41) leads to

$$F_n(t)=\zeta_n\int_0^l f_0 t\begin{pmatrix}\delta\left(x-\frac{l}{2}\right)\\ -(\mu)\delta''\left(x-\frac{l}{2}\right)\end{pmatrix}U_n(x)dx=\zeta_n f_0 t\left(U_n\left(\frac{l}{2}\right)-(\mu)U_n''\left(\frac{l}{2}\right)\right) \quad (44)$$

The mode shape and the second derivative of it at point $x=l/2$ in Eqs. (35) and (36) change into the following statements.

$$U_n\left(\frac{l}{2}\right)=\sqrt{\frac{2}{l}}sin\left(\frac{Pl}{2}\right) \quad (45)$$

$$U_n\left(\frac{l}{2}\right)=\sqrt{\frac{2}{l}}sin\left(\frac{Pl}{2}\right) \quad (46)$$

By applying Eqs. (45) and (46) into Eq. (44), the time-dependent concentrated force can be written in the following form.

$$F_n(t)=\sqrt{\frac{2}{l}}\zeta_n f_0 t\,sin\left(\frac{Pl}{2}\right)(1+(\mu)P^2) \quad (47)$$

Subsequently, the time-dependent generalized co-ordinates for linear loading can be rewritten as

$$\eta_n(t)=\alpha_n\int_0^t \tau sin\lambda_n(t-\tau)d\tau=\alpha_n\left(t-\frac{1}{\lambda_n}sin\,\lambda_n\,t\right) \quad (48)$$

where the coefficient α_n can be found as

$$\alpha_n=\frac{\zeta_n f_0\sqrt{\frac{2}{l}}sin\left(\frac{Pl}{2}\right)(1+(\mu)P^2)}{\lambda_n^2} \quad (49)$$

The axial displacement of Eq. (29) can be rewritten.

$$u(x,t)=\frac{f_0}{\rho A}\sum_{n=1}^{\infty}\frac{U_n(x_0)U_n(x_0)}{{\lambda_n}^2}\times\left(t-\frac{1}{\lambda_n}sin\,\lambda_n\,t\right) \quad (50)$$

Because the external force is concentrated at point $x=l/2$, the multiplication of the mode shapes for clamped-clamped boundary condition can be expressed as

$$U_n\left(\frac{l}{2}\right)\times U_n\left(\frac{l}{2}\right)=\begin{cases}0 & n=0\\ 2 & \\ l & n=1,3,5,\dots\end{cases} \quad (51)$$

Consequently, the axial displacement for the clamped-clamped boundary condition can be found as

$$u(x,t)=\frac{2f_0}{\rho Al}\sum_{n=1,3,5,..}^{\infty}\frac{1}{\lambda_n^2}\left(t-\frac{1}{\lambda_n}sin\,\lambda_n\,t\right) \quad (52)$$

Considering the clamped-free boundary condition, the multiplication of the mode shapes at point $x=l/2$ results in

$$U_n\left(\frac{l}{2}\right)\times U_n\left(\frac{l}{2}\right)=\begin{cases}0 & n=0\\ 1 & \\ l & n=1,2,3,\dots\end{cases} \quad (53)$$

By utilizing Eqs. (52), (53) and (29), the axial displacement can be rewritten as

$$u(x,t)=\frac{f_0}{\rho Al}\sum_{n=1}^{\infty}\frac{1}{\lambda_n^2}\left(t-\frac{1}{\lambda_n}sin\,\lambda_n\,t\right) \quad (54)$$

3.2.2 Harmonic axial concentrated force

This time, the time-dependent concentrated force is harmonic, and like the former loading is located at point $x=l/2$. Therefore, $f(x,t)$ can be rewritten as

$$f(x,t)=F_n(t)\delta\left(x-\frac{l}{2}\right)=(f_0\,sin\,\Omega\,t)\delta\left(x-\frac{l}{2}\right) \quad (55)$$

in which Ω expresses the excitation frequency. The time-dependent concentrated force for harmonic loading can be written as

$$\begin{aligned}F_n(t)&=\zeta_n\int_0^l f_0\,sin\,\Omega\,t\\ &\quad\times\left(\delta\left(x-\frac{l}{2}\right)-(\mu)\delta''\left(x-\frac{l}{2}\right)\right)\Theta_n(x)dx\\ &=\zeta_n f_0\,sin\,\Omega\,t\left(\Theta_n\left(\frac{l}{2}\right)-(\mu)\Theta_n''\left(\frac{l}{2}\right)\right)\end{aligned} \quad (56)$$

By using Eqs. (45) and (46), the time-dependent concentrated force can be simplified as

$$F_n(t)=\sqrt{\frac{2}{l}}\zeta_n f_0(sin\,\Omega\,t)\,sin\left(\frac{Pl}{2}\right)(1+(\mu)P^2) \quad (57)$$

The time-dependent generalized coordinates for harmonic loading can be stated as

$$\begin{aligned}\eta_n(t)&=\alpha_n\int_0^t(sin\,\Omega\,\tau)\,sin\,\lambda_n(t-\tau)d\tau\\ &=\alpha_n\left(sin\,\Omega\,t-\frac{\Omega}{\lambda_n}sin\,\lambda_n\,t\right)\end{aligned} \quad (58)$$

where the equivalent of α_n can be expressed as

$$\alpha_n=\frac{\sqrt{\frac{2}{l}}\zeta_n f_0\,sin\left(\frac{Pl}{2}\right)(1+(\mu)P^2)}{\lambda_n^2-\Omega^2} \quad (59)$$

The axial displacement for the harmonic loading can be defined as

$$u(x,t)=\frac{f_0}{\rho A}\sum_{n=1}^{\infty}\frac{U_n(x)U_n(x)}{(\lambda_n^2-\Omega^2)}\times\left(sin\,\Omega\,t-\frac{\Omega}{\lambda_n}sin\,\lambda_n\,t\right) \quad (60)$$

Considering that the concentrated axial force occurs at point $x=l/2$, and assuming the clamped-clamped boundary condition, substituting Eq. (51) into Eq. (60) leads to

$$u(x,t)=\frac{2f_0}{\rho Al}\sum_{n=1,3,5,..}^{\infty}\frac{\left(sin\,\Omega\,t-\frac{\Omega}{\lambda_n}sin\,\lambda_n\,t\right)}{(\lambda_n^2-\Omega^2)} \quad (61)$$

Based on Eq. (53) in which axial force concentrated at point $x=l/2$, Eq. (60) related to the axial displacement for clamped-free boundary condition can be rewritten as

$$u(x,t)=\frac{f_0}{\rho Al}\sum_{n=1}^{\infty}\frac{\left(sin\,\Omega\,t-\frac{\Omega}{\lambda_n}sin\,\lambda_n\,t\right)}{(\lambda_n^2-\Omega^2)} \quad (62)$$

4. Rayleigh theory

The equation of motion can be stated as (Hosseini *et al*. 2019)

$$\begin{aligned}&-\rho A\frac{\partial^2 u}{\partial t^2}+\rho\upsilon^2 I_p\frac{\partial^4 u}{\partial x^2\partial t^2}+f(x,t)+EA\frac{\partial^2 u}{\partial x^2}\\ &+\mu\left(\rho A\frac{\partial^4 u}{\partial x^2\partial t^2}-\rho\upsilon^2 I_p\frac{\partial^6 u}{\partial x^4\partial t^2}-\frac{\partial^2 f(x,t)}{\partial x^2}\right)=0\end{aligned} \quad (63)$$

where υ denotes the Poisson's ratio. To solve the above equation analytically, the discretized axial displacement in Eq. (29) can be employed in Eq. (63) to obtain the following equation

$$\begin{aligned}&\left(\rho A+\rho\upsilon^2 I_p P^2\right)\times(1+\mu P^2)\ddot{\eta}_n(t)+EAP^2\eta_n(t)\\ &=\left(f(x,t)-\frac{\partial^2 f(x,t)}{\partial x^2}\right)\end{aligned} \quad (64)$$

Eq. (64) can be simplified as

$$\ddot{\eta}_n(t) + {\lambda_{nR}}^2 \eta_n(t) = \zeta_{nR} F_n(t) \tag{65}$$

Based on Eq. (64), these coefficients are achievable as

$$\lambda_{nR} = \sqrt{\frac{EAP^2}{(1+\mu(P)^2)\left(\rho A + \rho v^2 I_p P^2\right)}} \tag{66}$$

$$\zeta_{nR} = \frac{1}{(1+\mu(P)^2)\left(\rho A + \rho v^2 I_p P^2\right)} \tag{67}$$

4.1 Linear concentrated axial load

Using Eqs. (48), (49), (66) and (67), the axial displacement in Eq. (29) for clamped-clamped boundary conditions can be obtained as

$$u(x,t) = \frac{2f_0}{l} \sum_{n=1,3,\ldots}^{\infty} \frac{\zeta_{nR}(1+\mu(P)^2)}{\lambda_{nR}^2} \times \left(t - \frac{1}{\lambda_{nR}} sin\,\lambda_{nR}\, t\right) \tag{68}$$

Also, the axial displacement using the same equation for clamped-free boundary condition can be calculated as

$$u(x,t) = \frac{f_0}{l} \sum_{n=1}^{\infty} \frac{\zeta_{nR}(1+\mu(P)^2)}{\lambda_{nR}^2} \times \left(t - \frac{1}{\lambda_{nR}} sin\,\lambda_{nR}\, t\right) \tag{69}$$

4.2 Harmonic concentrated axial load

By substituting Eqs. (58) and (59) into Eq. (29), and using Eqs. (66) and (67), the axial displacement for clamped-clamped boundary conditions is given by

$$u(x,t) = \frac{2f_0}{l} \times \sum_{n=1,3,5,..}^{\infty} \frac{\zeta_{nR}(1+\mu(P)^2) \times \left(sin\,\Omega\, t - \frac{\Omega}{\lambda_{nR}} sin\,\lambda_{nR}\, t\right)}{(\lambda_{nR}^2 - \Omega^2)} \tag{70}$$

Moreover, the axial displacement using the same equations for clamped-free boundary condition can be expressed as

$$u(x,t) = \frac{f_0}{l} \times \sum_{n=1}^{\infty} \frac{\zeta_{nR}(1+\mu(P)^2) \times \left(sin\,\Omega\, t - \frac{\Omega}{\lambda_{nR}} sin\,\lambda_{nR}\, t\right)}{(\lambda_{nR}^2 - \Omega^2)} \tag{71}$$

5. Bishop theory

The governing equation based on Bishop theory (Karličić *et al*. 2019) can be stated as

$$-\rho A \frac{\partial^2 u}{\partial t^2} + \rho v^2 I_p \frac{\partial^4 u}{\partial x^2 \partial t^2} - G v^2 I_p \frac{\partial^4 u}{\partial x^4} + f(x,t) + EA\frac{\partial^2 u}{\partial x^2} + \mu\left(\rho A(1+2v)\frac{\partial^4 u}{\partial x^2 \partial t^2} - \rho v^2 I_p \frac{\partial^6 u}{\partial x^4 \partial t^2} - \frac{\partial^2 f(x,t)}{\partial x^2}\right) = 0 \tag{72}$$

Applying Eq. (29) into Eq. (72) leads to

$$\left(\rho A(1+(1+2v)P^2\mu) + \rho v^2 I_p P^2(1+\mu P^2)\right)\ddot{\eta}_n(t) + \left(G v^2 I_p P^4 + EAP^2\right)\eta_n(t) = \left(f(x,t) - \frac{\partial^2 f(x,t)}{\partial x^2}\right) \tag{73}$$

Eq. (73) can be simplified as

$$\ddot{\eta}_n(t) + {\lambda_{nB}}^2 \eta_n(t) = \zeta_{nB} F_n(t) \tag{74}$$

Considering Eq. (74), the coefficient in Eq. (38) based on Bishop theory for a carbon nanotube are achievable as

$$\lambda_{nB} = \sqrt{\frac{G v^2 I_p P^4 + EAP^2}{\rho A(1+(1+2v)P^2\mu) + \rho v^2 I_p P^2(1+\mu P^2)}} \tag{75}$$

$$\zeta_{nB} = \frac{1}{\rho A(1+(1+2v)P^2\mu) + \rho v^2 I_p P^2(1+\mu P^2)} \tag{76}$$

5.1 Linear concentrated axial force

The axial displacement for clamped-clamped SWCNT by establishing Eqs. (48), (49), (75) and (76) into Eq. (29) can be rewritten as

$$u(x,t) = \frac{2f_0}{l} \sum_{n=1,3,5,..}^{\infty} \frac{\zeta_{nB}(1+\mu(P)^2)}{\lambda_{nB}^2}\left(t - \frac{1}{\lambda_{nB}} sin\,\lambda_{nB}\, t\right) \tag{77}$$

The axial displacement for clamped-free boundary condition is given by

$$u(x,t) = \frac{f_0}{l} \sum_{n=1}^{\infty} \frac{\zeta_{nB}(1+\mu(P)^2)}{\lambda_{nB}^2}\left(t - \frac{1}{\lambda_{nB}} sin\,\lambda_{nB}\, t\right) \tag{78}$$

5.2 Harmonic concentrated axial load

The axial displacement for clamped-clamped SWCNT can be rewritten as

$$u(x,t) = \frac{2f_0}{l} \sum_{n=1,3,5,..}^{\infty} \frac{\zeta_{nB}(1+\mu(P)^2) \times \left(sin\,\Omega\, t - \frac{\Omega}{\lambda_{nB}} sin\,\lambda_{nB}\, t\right)}{(\lambda_{nB}^2 - \Omega^2)} \tag{79}$$

Finally, the axial displacement for clamped-free SWCNT can be expressed as

$$u(x,t) = \frac{f_0}{l} \sum_{n=1}^{\infty} \frac{\zeta_{nB}(1+\mu(P)^2) \times \left(sin\,\Omega\, t - \frac{\Omega}{\lambda_n} sin\,\lambda_{nB}\, t\right)}{(\lambda_{nB}^2 - \Omega^2)} \tag{80}$$

Table 1 Geometrical and mechanical properties of SWCNT (Askari and Esmailzadeh 2017)

r (nm)	t (nm)	E (Gpa)	ρ (kg/m^3)	υ
1.37	0.34	933.061	2300	0.19

Table 2 Comparison of the first three non-dimensional frequency $\left[\omega_n \times l \times \sqrt{\rho/E}\right]$ of SWCNT based on the classical elasticity theory ($e_0 a = 0$) for two different boundary conditions

Mode	Ref. (Aydogdu 2012)		Present	
	CC	CF	CC	CF
1	3.14159	1.5708	3.141	1.570
2	6.28319	4.71239	6.283	4.712
3	9.42478	7.85398	9.424	7.853

Table 3 Comparison of the first three non-dimensional frequency $\left[\omega_n \times l \times \sqrt{\rho/E}\right]$ of SWCNT based on nonlocal elasticity theory ($e_0 a = 1$ nm) for two different boundary conditions

Mode	Ref. (Aydogdu 2012)		Present	
	CC	CF	CC	CF
1	2.99717	1.55177	2.997	1.551
2	5.32018	4.26279	5.320	4.262
3	6.85867	6.17668	6.858	6.176

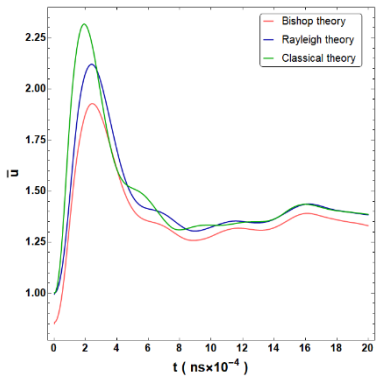

(a) $e_0 a = 1$ nm

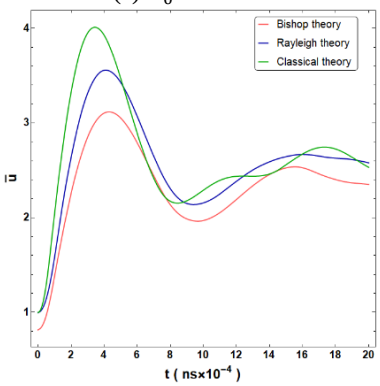

(b) $e_0 a = 2$ nm

Fig. 3 Variation of the non-dimensional axial displacement versus time for two different values of nonlocal parameters based on three different theories for clamped-clamped boundary condition under the linear concentrated force ($f_0 = 10^{12}$ nN/(ns × nm) and $l = 14.757$ nm)

6. Results and discussion

In this stage, the comparison between the obtained results of this study and available results has been done. The relations derived in the previous sections are used to investigate the non-dimensional natural frequencies firstly and then the dynamic axial displacements under the linear and harmonic concentrated force. The effects of the excitation frequency, length, nonlocal parameter and CNT's thickness also are explained in detail. Geometrical and mechanical properties used in this study are brought in Table 1 where r, l, t, ρ and υ represent the average radius, length, thickness, density of the SWCNT and Poisson's ratio with zigzag structure. Also, E denotes the Young's modulus.

It is necessary to have the inner and outer radii of the CNT to calculate the area of it. In this study, these amounts are equivalent to 1.2 nm and 1.54 nm, respectively.

In this part, the free axial vibration of the SWCNT in two different boundary conditions is investigated parametrically for classical elasticity theory and the nonlocal elasticity theory for $e_0 a = 1$ nm. The length is considered $l = 10$ nm. In Tables 2 and 3, the non-dimensional natural frequencies in the first three modes based on the classical elasticity theory for two different states of the boundary conditions are investigated. In Table 2, the nonlocal parameter is set to be zero, but in Table 3 is equal to $e_0 a = 1$ nm. It is seen that as the values of modes increase, the frequency enhances regardless of the type of the boundary condition. The effect of the non-locality is indicated in Table 3. It is obvious that the existence of the nonlocal parameters and subsequently raising in its amount, makes the natural frequency decrease due to the decrement in stiffness. Good agreement is observed between obtained and reference results in both tables.

Figs. 3-5 demonstrate the dimensional and non-dimensional axial displacements for clamped-clamped SWCNT when a linear time-dependent force is exerted at the midpoint of the CNT (i.e., $x = l/2$) for three various theories, including Bishop, Rayleigh, and classical theories. In Figs. 3(a) and (b), the variations of the non-dimensional axial displacement versus time are demonstrated. By increasing the nonlocal parameter, the effective stiffness of the CNT decreases, and consequently, the axial displacement increases. In contrast, the axial displacement increases by the steep slope first and then decreases almost with the same slope and vibrates with constant wavelengths and amplitudes. For the case $e_0 a = 2$ nm, the behavior of the vibration is the same except that the values of the axial displacement, as well as the wavelength, are more than the case $e_0 a = 1$ nm. Also, it is comprehensible that the axial displacements disregarding the type of the used theory get

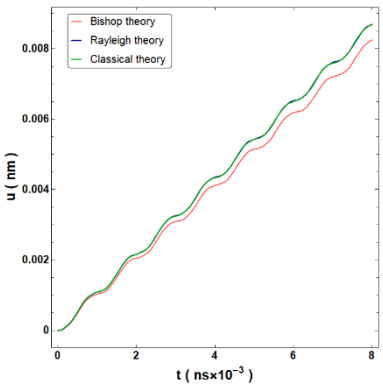

(a) $l = 10$ nm

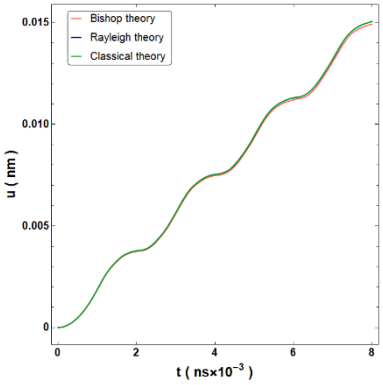

(b) $l = 20$ nm

Fig. 4 The comparison of the axial displacement versus time for two different values of lengths based on three different theories under the linear concentrated force for clamped-clamped boundary condition as well as $e_0 a = 0.5$ nm and constant amplitude $f_0 = 10^{12}$ nN/(ns × nm)

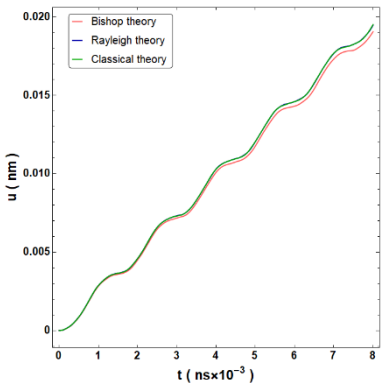

(a) $t = 0.2$ nm

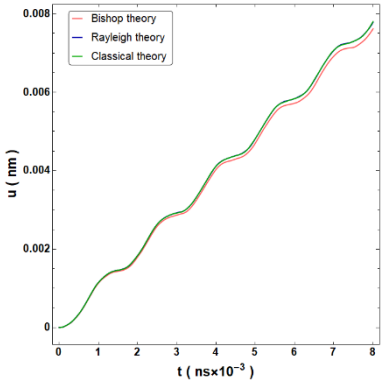

(b) $t = 0.5$ nm

Fig. 5 The comparison of the axial displacement versus time for two different values of thicknesses based on three different theories under the linear concentrated force for clamped-clamped boundary condition ($e_0 a = 0.5$ nm, l =14.757 nm and $f_0 = 10^{12}$ nN/(ns × nm))

closer together for the lower values of the nonlocal parameters. Among the theories, Rayleigh and classical theories will be consistent after the first maximum point. The variation of the axial displacements versus time for two values of lengths (i.e., $l = 10$ nm and $l = 20$ nm) are investigated in Figs. 4(a) and (b), respectively. It is obvious, the value of the length increases by the time due to the linear time-dependent axial force. The value of the length has a direct effect on the axial displacement. Also, the axial displacement for various theories will be approximately same for greater values of the lengths, while for $l = 10$ nm, the value of the axial displacements for Rayleigh and classical theory similarly increases over time. Again, the axial displacement for Bishop theory is less than the other theories. Figs. 5(a) and (b) indicate the variation of the axial displacement for two various thicknesses. As it was expectable, the value of the axial displacement reduces by the enhancement of the value of the thickness, and the rate of this reduction decreases as the value of the thickness grows. The axial displacement grows with an approximately constant slope. It also can be concluded that for the different values of the thicknesses, the values of the axial displacement are similar for Rayleigh and classical theories, and the difference between the slope of the plot for these theories and Bishop theory is independent of the values of the thicknesses. Figs. 6-8 demonstrate the dimensional and non-dimensional axial displacements for clamped-free SWCNT subjected to a linear time-dependent force at the midpoint of the CNT for three mentioned theories.

Figs. 6(a) and (b) are almost similar to Figs. 3(a) and (b), respectively. The difference is that after the first period for the C-F boundary condition, the axial displacement will possess lower amounts. Afterward, the amplitude of the vibration will be lower in comparison with C-C one. Figs. 7(a) and (b) show the axial displacement in the time domain. The plots have been indicated for two various values of lengths. By the increment of the value of the length, all three theories behave completely the same through time. Also, the axial displacement and wavelength increase by an increase in the value of the length. Again, the behavior of the vibration is similar to Rayleigh and classical theories. The variations of the axial displacement versus time have been demonstrated through two figures for two various thicknesses in Figs. 8(a) and (b). It is distinctly clear that the slope of the plot and totally the value of the axial displacement decrease by the increase of the thickness. The value of the axial displacement is lower for clamped-clamped boundary condition in comparison with clamped-free one. Because, the free side in C-F SWCNT leads more freedom of the action, and as a result, it needs lower time to

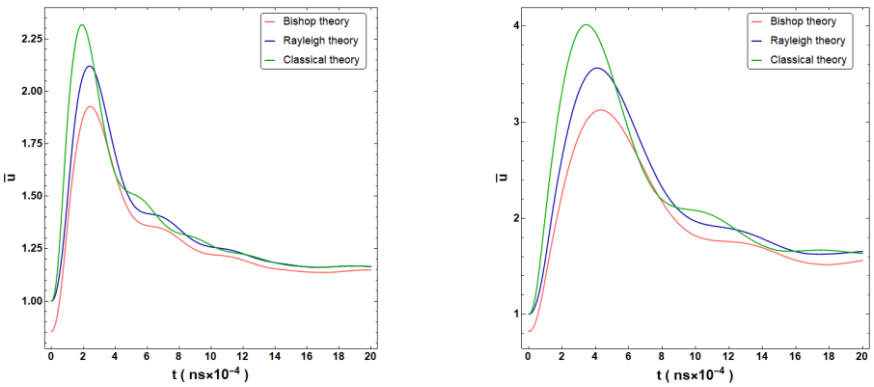

(a) $e_0a = 1$ nm (b) $e_0a = 2$ nm

Fig. 6 The comparison of the non-dimensional axial displacement versus time for two different values of nonlocal parameters based on three different theories under the linear concentrated force for clamped-free boundary condition (l =14.757 nm and $f_0 = 10^{12}$ nN/(ns × nm)

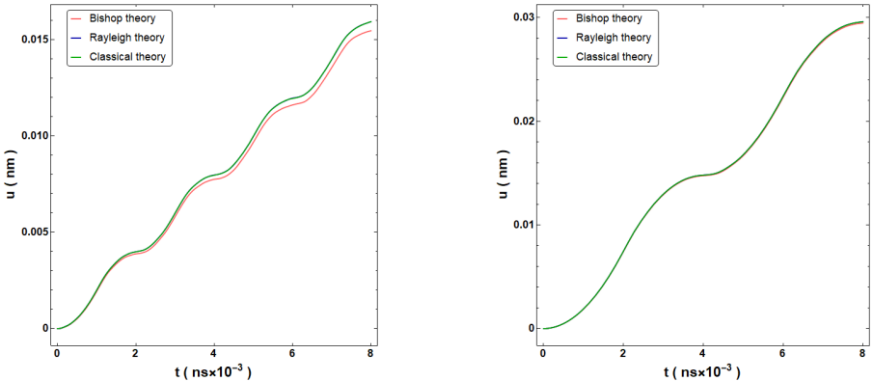

(a) $l = 10$ nm (b) $l = 20$ nm

Fig. 7 The comparison of the axial displacement versus time for two different values of lengths based on three different theories under the linear concentrated force for clamped-free boundary conditions, $e_0a = 0.5$ nm and $f_0 = 10^{12}$ nN/(ns × nm)

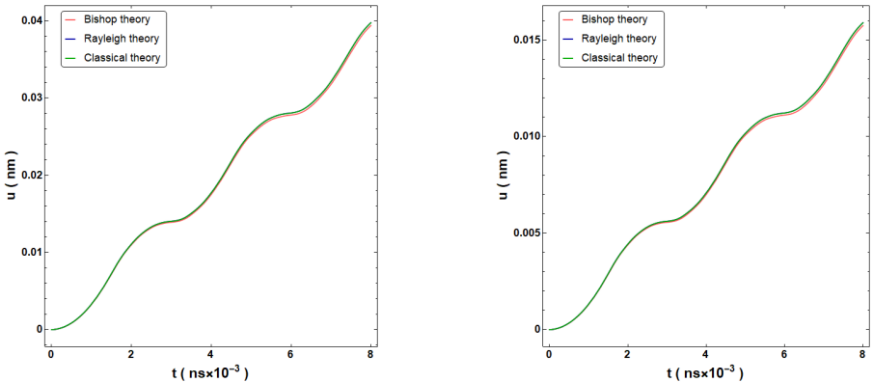

(a) $t = 0.2$ nm (b) $t = 0.5$ nm

Fig. 8 The comparison of the axial displacement versus time for two different values of thicknesses based on three different theories under the linear concentrated force for clamped-free boundary condition ($e_0a = 0.5$ nm, $l = 14.757$ nm and $f_0 = 10^{12}$nN/(ns × nm)

reach a specified axial displacement.

Figs. 9-11 depict the variation of the non-dimensional and dimensional axial displacement in the time domain for a clamped-clamped SWCNT subjected to a harmonic axial force for three mentioned theories. The non-dimensional axial displacement in the time domain has been indicated in Figs. 9(a) and (b), which exactly are similar to Figs. 3(a) and (b). The variation of the axial displacement versus time

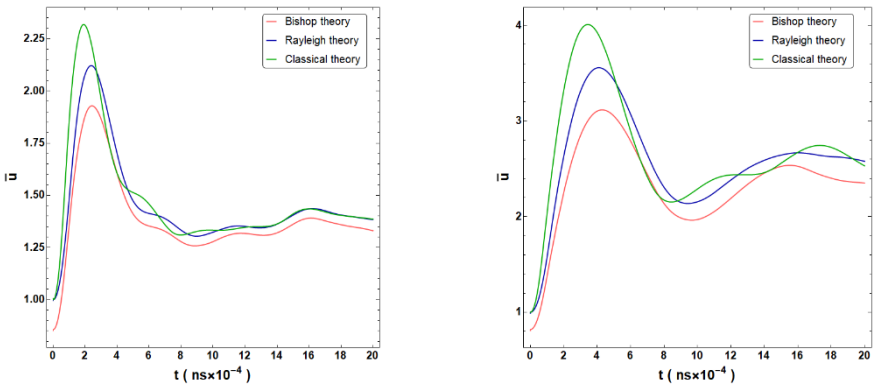

(a) $e_0a = 1$ nm (b) $e_0a = 2$ nm

Fig. 9 The comparison of the non-dimensional axial displacement versus time for two different values of nonlocal parameters based on three different theories under the harmonic concentrated force for clamped-clamped boundary condition ($f_0 = 10$ nN/ns, $l = 14.757$ nm and excitation frequency $\Omega = 4 \times 10^{10}$)

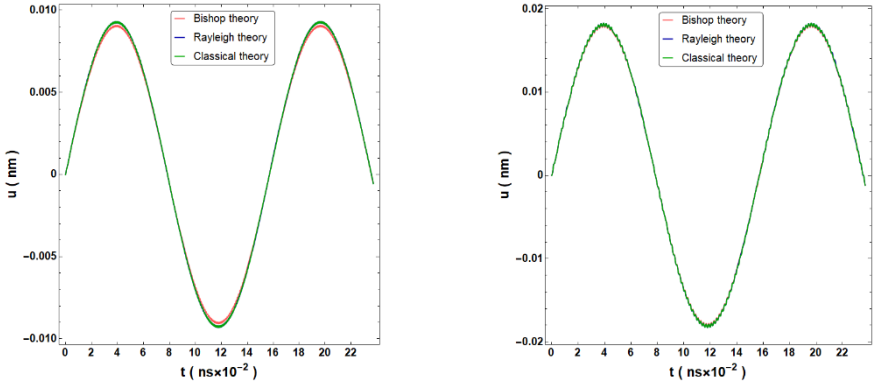

(a) $l = 10$ nm (b) $l = 20$ nm

Fig. 10 The comparison of the axial displacement versus time for two different values of lengths based on three different theories for clamped-clamped boundary condition under the linear concentrated force for ($f_0 = 10$ nN/ns, $e_0a = 0.2$ nm and $\Omega = 4 \times 10^{10}$)

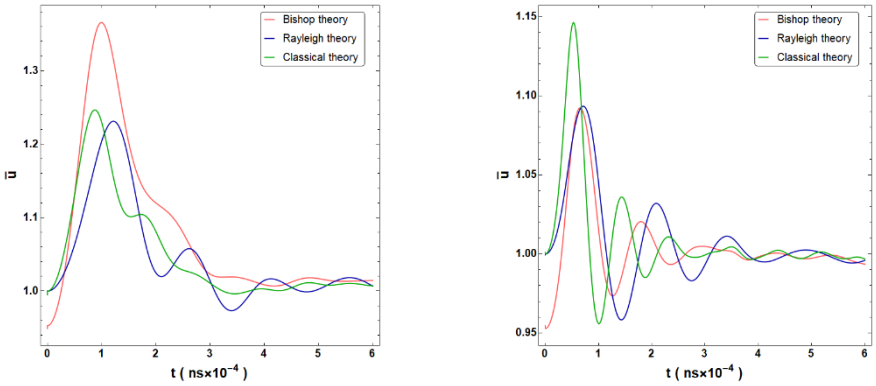

(a) $\Omega = 0.2\omega_n$ (b) $\Omega = 2\omega_n$

Fig. 11 The comparison of the axial displacement versus time for two different values of excitation frequency based on three different theories under the harmonic concentrated force for clamped-clamped boundary condition ($f_0 = 10$ nN/ns, $l = 14.757$ nm and $e_0a = 0.2$ nm)

has been illustrated in Figs. 10(a) and (b) for two different values of the length. As can be seen, the axial displacement for each theory has exactly similar behavior. Thus, an increase in length leads to be in accordance with the results based on utilized theories, and the length has a direct effect on the value of the non-dimensional axial displacement. The effect of the excitation frequency to natural frequency ratio (Ω/ω_n) has been shown in the form of Figs. 11(a) and

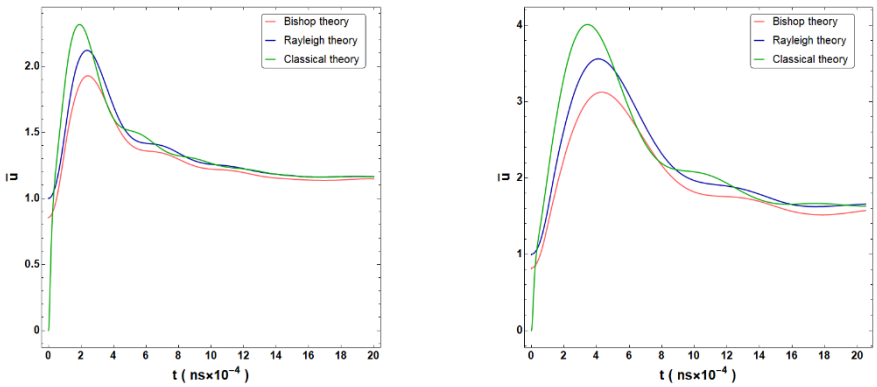

(a) $e_0 a = 1$ nm (b) $e_0 a = 2$ nm

Fig. 12 The comparison of the non-dimensional axial displacement versus time for two different values of nonlocal parameters based on three different theories under the harmonic concentrated force for clamped-free boundary condition ($f_0 = 10$ nN/ns, $l = 14.757$ nm and $\Omega = 4 \times 10^{10}$)

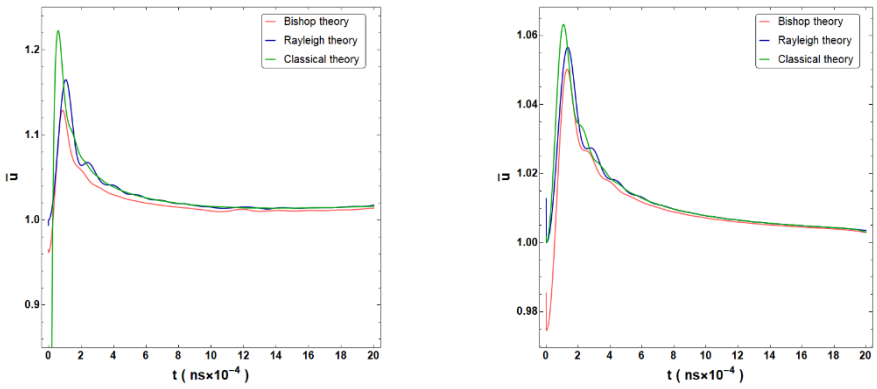

(a) $l = 10$ nm (b) $l = 20$ nm

Fig. 13 The comparison of the non-dimensional axial displacement versus time for two different values of lengths based on three different theories under the harmonic concentrated force for clamped-free boundary condition ($f_0 = 10$ nN/ns, $e_0 a = 0.2$ nm and $\Omega = 4 \times 10^{10}$)

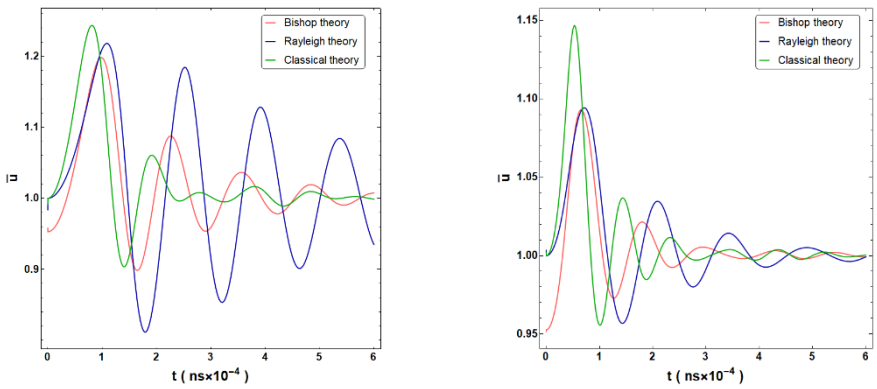

(a) $\Omega = 0.5\omega_n$ (b) $\Omega = 2\omega_n$

Fig. 14 Variation of the axial displacement versus time for two different values of excitation frequency based on three different theories under the harmonic concentrated force for clamped-free boundary condition ($f_0 = 10$ nN/ns, $l = 14.757$ nm and $e_0 a = 0.2$ nm)

(b). It is clear that by an increase in the ratio, the axial displacement decreases. Also, the non-dimensional axial displacement has the maximum amount in the first period for Bishop theory in Fig. 11(a), while the maximum values occur for classical theory in Fig. 11(b). Figs. 12-14 plot the non-dimensional axial displacement versus time for clamped-free boundary condition for harmonic loading. The behavior of the Fig. 12 is consistent with Fig. 6 for different

nonlocal parameters. The variations of the non-dimensional axial displacement in the time domain have been indicated in Figs. 13(a) and (b). The non-dimensional axial displacement decreases by the increment of the length, while the axial displacement increases by the increment of the length. After the first period, the axial displacement continues at a constant rate. Figs. 14(a) and (b) depict the excitation frequency to natural frequency ratio effect on the non-dimensional axial displacement. As it is clear, the axial displacement decreases by raising the excitation frequency to the natural frequency ratio. The maximum point decreases by a greater rate for classical theory in both cases, while this reduction has a lower rate based on the Rayleigh theory.

7. Conclusions

Free axial vibration along with the dynamic forced axial vibration analysis was established in SWCNT with a zigzag structure based on Eringen's nonlocal elasticity (classical theory), Rayleigh and Bishop theories. The constitutive relations were used to derive the equation of motion and boundary conditions. The derived governing equations solved by an analytical method. The results were investigated for C-C and C-F boundary conditions. It was shown that in the time-dependent forced axial vibration, the nonlocal parameter has a direct effect on the variation of the non-dimensional and dimensional axial displacements disregarding the type of the loading and boundary conditions. The length has a direct effect on axial displacement but has an inverse effect on the non-dimensional axial displacement. Also, the thickness, as well as the excitation to natural frequency ratio, have inverse effects on the variation of the axial displacement for every type of loading and boundary conditions. Among the applied theories, classical and Rayleigh theories are closer together. The value of the axial displacement based on Bishop theory is lower than the two other theories except when the excitation frequency to the natural frequency ratio is less than one, and the harmonic loading on the C-C SWCNT is applied. Furthermore, contrary to the increase in thickness, an increase in the length causes the wavelength to increase. In the non-dimensional state, the behavior of the vibration for the same loadings, boundary conditions and parameters are the same. When the effect of the excitation frequency to natural frequency ratio is taken into account, whether the C-C or C-F boundary condition is applied, and whether the ratio is greater or lower than one, the value of the axial displacement reduces with the lower rate based on the Bishop theory. The axial displacement for the C-F boundary condition is greater than C-C one.

References

Adams, F.C. and Barbante, C. (2013), "Nanoscience, nanotechnology and spectrometry", *Spectrochim. Acta Part B At. Spectrosc.*, **86**, 3-13. https://doi.org/10.1016/j.sab.2013.04.008.

Ajayan, P.M. (1999), "Nanotubes from carbon", *Chem. Rev.*, **99**(7), 1787-1800. https://doi.org/10.1021/cr970102g.

Akbaş, Ş.D. (2018), "Forced vibration analysis of cracked functionally graded microbeams", *Adv. Nano Res., Int. J.*, **6**(1), 39-55. https://doi.org/10.12989/anr.2018.6.1.039.

Alizadeh Hamidi, B., Hosseini, S.A., Hassannejad, R. and Khosravi, F. (2020), "An exact solution on gold microbeam with thermoelastic damping via generalized Green-Naghdi and modified couple stress theories", *J. Therm. Stress.*, **43**(2), 157-174. https://doi.org/10.1080/01495739.2019.1666694.

Askari, H. and Esmailzadeh, E. (2017), "Forced vibration of fluid conveying carbon nanotubes considering thermal effect and nonlinear foundations", *Compos. Part B Eng.*, **113**, 31-43. https://doi.org/10.1016/j.compositesb.2016.12.046.

Aydogdu, M. (2009), "Axial vibration of the nanorods with the nonlocal continuum rod model", *Physica E Low Dimens. Syst. Nanostruct.*, **41**(5), 861-864. https://doi.org/10.1016/j.physe.2009.01.007.

Aydogdu, M. (2012), "Axial vibration analysis of nanorods (carbon nanotubes) embedded in an elastic medium using nonlocal elasticity", *Mech. Res. Commun.*, **43**, 34-40. https://doi.org/10.1016/j.mechrescom.2012.02.001.

Aydogdu, M. (2015), "A nonlocal rod model for axial vibration of double-walled carbon nanotubes including axial van der Waals force effects", *J. Vib. Control.*, **21**(16), 3132-3154. https://doi.org/10.1177/1077546313518954.

Aydogdu, M. and Filiz, S. (2011), "Modeling carbon nanotube-based mass sensors using axial vibration and nonlocal elasticity", *Physica E Low Dimens. Syst. Nanostruct.*, **43**(6), 1229-1234. https://doi.org/10.1016/j.physe.2011.02.006.

Bastanfar, M., Hosseini, S.A., Sourki, R. and Khosravi, F. (2019), "Flexoelectric and surface effects on a cracked piezoelectric nanobeam: Analytical resonant frequency response", *Arch. Mech. Eng.*, **66**(4), 417-437. https://doi.org/10.24425/ame.2019.131355.

Bensaid, I., Bekhadda, A. and Kerboua, B. (2018), "Dynamic analysis of higher order shear-deformable nanobeams resting on elastic foundation based on nonlocal strain gradient theory", *Adv. Nano Res., Int. J.*, **6**(3), 279-298. http://dx.doi.org/10.12989/anr.2018.6.3.279.

Bethune, D., Kiang, C.H., De Vries, M., Gorman, G., Savoy, R., Vazquez, J. and Beyers, R. (1993), "Cobalt-catalysed growth of carbon nanotubes with single-atomic-layer walls", *Nature*, **363**(6430), 605-607. https://doi.org/10.1038/363605a0.

Bianco, A., Kostarelos, K., Partidos, C.D. and Prato, M. (2005), "Biomedical applications of functionalised carbon nanotubes", *Chem. Commun.*, **1**(5), 571-577. https://doi.org/10.1039/B410943K.

Boutaleb, S., Benrahou, K.H., Bakora, A., Algarni, A., Bousahla, A.A., Tounsi, A., Tounsi, A. and Mahmoud, S. (2019), "Dynamic analysis of nanosize FG rectangular plates based on simple nonlocal quasi 3D HSDT", *Adv. Nano Res., Int. J.*, **7**(3), 191-208. http://dx.doi.org/10.12989/anr.2019.7.3.191.

Caruthers, S.D., Wickline, S.A. and Lanza, G.M. (2007), "Nanotechnological applications in medicine", *Curr. Opin. Biotechnol.*, **18**(1), 26-30. https://doi.org/10.1016/j.copbio.2007.01.006.

Chau, R., Datta, S., Doczy, M., Doyle, B., Jin, B., Kavalieros, J., Majumdar, A., Metz, M. and Radosavljevic, M. (2005), "Benchmarking nanotechnology for high-performance and low-power logic transistor applications", *IEEE Trans. Nanotechnol.*, **4**(2), 153-158. https://doi.org/10.1109/TNANO.2004.842073.

Cox, B.J., Thamwattana, N. and Hill, J.M. (2008), "Mechanics of nanotubes oscillating in carbon nanotube bundles", *Proc. Math. Phys. Eng. Sci.*, **464**(2091), 691-710. https://doi.org/10.1098/rspa.2007.0247.

Dai, H. (2002), "Carbon nanotubes: Opportunities and challenges", *Surf. Sci.*, **500**(1-3), 218-241.

https://doi.org/10.1016/S0039-6028(01)01558-8.
Danesh, M., Farajpour, A. and Mohammadi, M. (2012), "Axial vibration analysis of a tapered nanorod based on nonlocal elasticity theory and differential quadrature method", *Mech. Res. Commun.*, **39**(1), 23-27. https://doi.org/10.1016/j.mechrescom.2011.09.004.
De Volder, M.F., Tawfick, S.H., Baughman, R.H. and Hart, A.J. (2013), "Carbon nanotubes: Present and future commercial applications", *Science*, **339**(6119), 535-539. https://doi.org/10.1126/science.1222453.
Diallo, M., Street, A., Sustich, R., Duncan, J. and Savage, N. (2009), *Nanotechnology Applications for Clean Water: Solutions for Improving Water Quality*, William Andrew, New York, USA.
Ebrahimi, F., Dehghan, M. and Seyfi, A. (2019), "Eringen's nonlocal elasticity theory for wave propagation analysis of magneto-electro-elastic nanotubes", *Adv. Nano Res., Int. J.*, **7**(1), 1-11. https://doi.org/10.12989/anr.2019.7.1.001.
Eltaher, M., Alshorbagy, A.E. and Mahmoud, F. (2013), "Vibration analysis of Euler–Bernoulli nanobeams by using finite element method", *Appl. Math. Model.*, **37**(7), 4787-4797. https://doi.org/10.1016/j.apm.2012.10.016.
Eringen, A.C. (1983), "On differential equations of nonlocal elasticity and solutions of screw dislocation and surface waves", *J. Appl. Phys.*, **54**(9), 4703-4710. https://doi.org/10.1063/1.332803.
Esawi, A.M. and Farag, M.M. (2007), "Carbon nanotube reinforced composites: potential and current challenges", *Mater. Des.*, **28**(9), 2394-2401. https://doi.org/10.1016/j.matdes.2006.09.022.
Georgantzinos, S. and Anifantis, N. (2010), "Carbon nanotube-based resonant nanomechanical sensors: A computational investigation of their behavior", *Physica E Low Dimens. Syst. Nanostruct.*, **42**(5), 1795-1801. https://doi.org/10.1016/j.physe.2010.02.002.
Glory, J., Bonetti, M., Helezen, M., Mayne-L'Hermite, M. and Reynaud, C. (2008), "Thermal and electrical conductivities of water-based nanofluids prepared with long multiwalled carbon nanotubes", *J. Appl. Phys.*, **103**(9), 094309. https://doi.org/10.1063/1.2908229.
Gooding, J.J. (2005), "Nanostructuring electrodes with carbon nanotubes: A review on electrochemistry and applications for sensing", *Electrochim. Acta*, **50**(15), 3049-3060. https://doi.org/10.1016/j.electacta.2004.08.052.
Hamidi, B.A., Hosseini, S.A., Hassannejad, R. and Khosravi, F. (2020), "Theoretical analysis of thermoelastic damping of silver nanobeam resonators based on Green-Naghdi via nonlocal elasticity with surface energy effects", *Eur. Phys. J. Plus*, **135**(1), 1-20. https://doi.org/10.1140/epjp/s13360-019-00037-8.
Harris, P.J. and Harris, P.J.F. (2009), *Carbon Nanotube Science: Synthesis, Properties and Applications*, Cambridge University Press, London, UK.
He, H., Pham-Huy, L.A., Dramou, P., Xiao, D., Zuo, P. and Pham-Huy, C. (2013), "Carbon nanotubes: Applications in pharmacy and medicine", *BioMed Res. Int.*, **2013**, 578290. https://doi.org/10.1155/2013/578290.
Hosseini, S.A. and Khosravi, F. (2020), "Exact solution for dynamic response of size dependent torsional vibration of CNT subjected to linear and harmonic loadings", *Adv. Nano Res., Int. J.*, **8**(1), 25-36. https://doi.org/10.12989/anr.2020.8.1.025.
Hosseini, S.A., Khosravi, F. and Ghadiri, M. (2019), "Moving axial load on dynamic response of single-walled carbon nanotubes using classical, Rayleigh and Bishop rod models based on Eringen's theory", *J. Vib. Control*, **26**(11-12), 913-928. https://doi.org/10.1177/1077546319890170.
Hosseini, S.A., Khosravi, F. and Ghadiri, M. (2020), "Effect of external moving torque on dynamic stability of carbon nanotube", *J. Nano Res.*, **61**, 118-135. https://doi.org/10.4028/www.scientific.net/JNanoR.61.118.
Iijima, S. (1991), "Helical microtubules of graphitic carbon", *Nature*, **354**(6348), 56-58. https://doi.org/10.1038/354056a0.
Iost, R.M. and Crespilho, F.N. (2012), "Layer-by-layer self-assembly and electrochemistry: Applications in biosensing and bioelectronics", *Biosens. Bioelectron.*, **31**(1), 1-10. https://doi.org/10.1016/j.bios.2011.10.040.
Joshi, M., Bhattacharyya, A. and Ali, S.W. (2008), "Characterization techniques for nanotechnology applications in textiles", *Indian J. Fibre Text. Res.*, **33**(3), 304-317.
Karaoglu, P. and Aydogdu, M. (2010), "On the forced vibration of carbon nanotubes via a non-local Euler-Bernoulli beam model", *Proc. Inst. Mech. Eng. C J. Mech. Eng. Sci.*, **224**(2), 497-503. https://doi.org/10.1243/09544062JMES1707.
Karličić, D.Z., Ayed, S. and Flaieh, E. (2019), "Nonlocal axial vibration of the multiple Bishop nanorod system", *Math. Mech. Solids.*, **24**(6), 1668-1691. https://doi.org/10.1177/1081286518766577.
Katariya, P.V. and Panda, S.K. (2019a), "Frequency and deflection responses of shear deformable skew sandwich curved shell panel: A finite element approach", *Arab. J. Sci. Eng.*, **44**(2), 1631-1648. https://doi.org/10.1007/s13369-018-3633-0.
Katariya, P.V. and Panda, S.K. (2019b), "Numerical evaluation of transient deflection and frequency responses of sandwich shell structure using higher order theory and different mechanical loadings", *Eng. Comput.*, **35**(3), 1009-1026. https://doi.org/10.1007/s00366-018-0646-y.
Katariya, P.V. and Panda, S.K. (2019c), "Numerical frequency analysis of skew sandwich layered composite shell structures under thermal environment including shear deformation effects", *Struct. Eng. Mech., Int. J.*, **71**(6), 657-668. https://doi.org/10.12989/sem.2019.71.6.657.
Katariya, P.V., Panda, S.K. and Mahapatra, T.R. (2017), "Prediction of nonlinear eigenfrequency of laminated curved sandwich structure using higher-order equivalent single-layer theory", *J. Sandw. Struct. Mater.*, **21**(8), 2846-2869. https://doi.org/10.1177/1099636217728420.
Katariya, P.V., Das, A. and Panda, S.K. (2018), "Buckling analysis of SMA bonded sandwich structure-using FEM", *Proceedings of the 7th National Conference on Processing and Characterization of Materials*, Roukela, India, December.
Kelly, B. (1981), *Physics of Graphite*, Applied Science, London, UK.
Khosravi, F. and Hosseini, S.A. (2020), "On the viscoelastic carbon nanotube mass nanosensor using torsional forced vibration and Eringen's nonlocal model", *Mech. Based Des. Struct. Mach.*, **2020**, 1-24. https://doi.org/10.1080/15397734.2020.1744001.
Khosravi, F., Hosseini, S.A. and Hamidi, B.A. (2020a), "On torsional vibrations of triangular nanowire", *Thin-Wall. Struct.*, **148**, 106591. https://doi.org/10.1016/j.tws.2019.106591.
Khosravi, F., Hosseini, S.A. and Hamidi, B.A. (2020b), "Torsional Vibration of nanowire with equilateral triangle cross section based on nonlocal strain gradient for various boundary conditions: comparison with hollow elliptical cross section", *Eur. Phys. J. Plus.*, **135**(3), 1-20. https://doi.org/10.1140/epjp/s13360-020-00312-z.
Khosravi, F., Hosseini, S.A. and Hayati, H. (2020c), "Free and forced axial vibration of single walled carbon nanotube under linear and harmonic concentrated forces based on nonlocal theory", *Int. J. Mod. Phys. B*, **34**(8), 2050067. https://doi.org/10.1142/S0217979220500678.
Khosravi, F., Hosseini, S.A. and Norouzi, H. (2020d), "Exponential and harmonic forced torsional vibration of single-walled carbon nanotube in an elastic medium", *Proc. Inst. Mech. Eng. C J. Mech. Eng. Sci.*, **234**(10), 1928-1942.

https://doi.org/10.1177/0954406220903341.

Khosravi, F., Hosseini, S.A. and Tounsi, A. (2020e), "Forced axial vibration of a single-walled carbon nanotube embedded in elastic medium under various moving forces", *J. Nano Res.*, **63**, 112-133. https://doi.org/10.4028/www.scientific.net/JNanoR.63.112.

Khosravi, F., Hosseini, S.A. and Tounsi, A. (2020f), "Torsional dynamic response of viscoelastic SWCNT subjected to linear and harmonic torques with general boundary conditions via Eringen's nonlocal differential model", *Eur. Phys. J. Plus*, **135**(2), 183. https://doi.org/10.1140/epjp/s13360-020-00207-z.

Kunche, M.C., Mishra, P.K., Nallala, H.B., Hirwani, C.K., Katariya, P.V., Panda, S. and Panda, S.K. (2019), "Theoretical and experimental modal responses of adhesive bonded T-joints", *Wind Struct., Int. J.*, **29**(5), 361-369. https://doi.org/10.12989/was.2019.29.5.361.

Lei, Z., Liew, K. and Yu, J. (2013), "Free vibration analysis of functionally graded carbon nanotube-reinforced composite cylindrical panels", *Int. J. Mater. Sci.*, **1**(1), 36-40. https://doi.org/0.12720/ijmse.1.1.36-40.

Li, C., Lim, C.W. and Yu, J. (2010), "Dynamics and stability of transverse vibrations of nonlocal nanobeams with a variable axial load", *Smart Mater. Struct.*, **20**(1), 015023. https://doi.org/10.1088/0964-1726/20/1/015023.

Liu, K.C., Friend, J. and Yeo, L. (2009), "The axial-torsional vibration of pretwisted beams", *J. Sound Vib.*, **321**(1-2), 115-136. https://doi.org/10.1016/j.jsv.2008.09.016.

Makar, J. and Beaudoin, J. (2004), "Carbon nanotubes and their application in the construction industry", *Proceedings of the 1st International Symposium on Nanotechnology in Construction*, Paisley, Scotland, June.

Mehar, K. and Panda, S.K. (2018a), "Thermal free vibration behavior of FG-CNT reinforced sandwich curved panel using finite element method", *Polym. Compos.*, **39**(8), 2751-2764. https://doi.org/10.1002/pc.24266.

Mehar, K. and Panda, S.K. (2018b), "Thermoelastic flexural analysis of FG-CNT doubly curved shell panel", *Aircr. Eng. Aerosp. Technol.*, **90**(1), 11-23. https://doi.org/10.1108/AEAT-11-2015-0237.

Mehar, K. and Panda, S.K. (2019), "Multiscale modeling approach for thermal buckling analysis of nanocomposite curved structure", *Adv. Nano Res., Int. J.*, **7**(3), 181-190. http://dx.doi.org/10.12989/anr.2019.7.3.181.

Mehar, K. and Panda, S.K. (2020), "Nonlinear deformation and stress responses of a graded carbon nanotube sandwich plate structure under thermoelastic loading", *Acta Mech.*, **231**(3), 1105-1123. https://doi.org/10.1007/s00707-019-02579-5.

Mehar, K., Panda, S.K. and Mahapatra, T.R. (2017a), "Theoretical and experimental investigation of vibration characteristic of carbon nanotube reinforced polymer composite structure", *Int. J. Mech. Sci.*, **133**, 319-329. https://doi.org/10.1016/j.ijmecsci.2017.08.057.

Mehar, K., Panda, S.K. and Patle, B.K. (2017b), "Thermoelastic vibration and flexural behavior of FG-CNT reinforced composite curved panel", *Int. J. Appl. Mech.*, **9**(4), 1750046. https://doi.org/10.1142/S1758825117500466.

Mehar, K., Mahapatra, T.R., Panda, S.K., Katariya, P.V. and Tompe, U.K. (2018a), "Finite-element solution to nonlocal elasticity and scale effect on frequency behavior of shear deformable nanoplate structure", *J. Eng. Mech.*, **144**(9), 04018094. https://doi.org/10.1061/(ASCE)EM.1943-7889.0001519.

Mehar, K., Panda, S.K. and Mahapatra, T.R. (2018b), "Nonlinear frequency responses of functionally graded carbon nanotube-reinforced sandwich curved panel under uniform temperature field", *Int. J. Appl. Mech.*, **10**(3), 1850028. https://doi.org/10.1142/S175882511850028X.

Mehar, K., Panda, S.K. and Patle, B.K. (2018c), "Stress, deflection, and frequency analysis of CNT reinforced graded sandwich plate under uniform and linear thermal environment: A finite element approach", *Polym. Compos.*, **39**(10), 3792-3809. https://doi.org/10.1002/pc.24409.

Mehralian, F. and Beni, Y.T. (2017), "A nonlocal strain gradient shell model for free vibration analysis of functionally graded shear deformable nanotubes", *Int. J. Eng. Appl. Sci.*, **9**(2), 88-102. http://dx.doi.org/10.24107/ijeas.309818.

Miyako, E., Hosokawa, C., Kojima, M., Yudasaka, M., Funahashi, R., Oishi, I., Hagihara, Y., Shichiri, M., Takashima, M. and Nishio, K. (2011), "A photo-thermal-electrical converter based on carbon nanotubes for bioelectronic applications", *Angew. Chem. Int. Ed.*, **50**(51), 12266-12270. https://doi.org/10.1002/anie.201106136.

Mohammadian, M., Abolbashari, M.H. and Hosseini, S.M. (2019), "Axial vibration of hetero-junction CNTs mass nanosensors by considering the effects of small scale and connecting region: An analytical solution", *Physica B Condens. Matter.*, **553**, 137-150. https://doi.org/10.1016/j.physb.2018.10.044.

Natsuki, T., Matsuyama, N., Shi, J.X. and Ni, Q.Q. (2014), "Vibration analysis of nanomechanical mass sensor using carbon nanotubes under axial tensile loads", *Appl. Phys. A*, **116**(3), 1001-1007. https://doi.org/10.1007/s00339-014-8289-3.

Oveissi, S., Toghraie, D. and Eftekhari, S.A. (2016), "Longitudinal vibration and stability analysis of carbon nanotubes conveying viscous fluid", *Physica E Low Dimens. Syst. Nanostruct.*, **83**, 275-283. https://doi.org/10.1016/j.physe.2016.05.004.

Panda, S.K. and Katariya, P.V. (2015), "Stability and free vibration behaviour of laminated composite panels under thermo-mechanical loading", *Int. J. Appl. Comput. Math.*, **1**(3), 475-490. https://doi.org/10.1016/j.physe.2016.05.004.

Pandey, H.K., Hirwani, C.K., Sharma, N., Katariya, P.V., Dewangan, H.C. and Panda, S.K. (2019), "Effect of nano glass cenosphere filler on hybrid composite eigenfrequency responses-An FEM approach and experimental verification", *Adv. Nano Res., Int. J.*, **7**(6), 419-429. https://doi.org/10.12989/anr.2019.7.6.419.

Paradise, M. and Goswami, T. (2007), "Carbon nanotubes-production and industrial applications", *Mater. Des.*, **28**(5), 1477-1489. https://doi.org/10.1016/j.matdes.2006.03.008.

Rahmani, O., Hosseini, S., Ghoytasi, I. and Golmohammadi, H. (2017), "Buckling and free vibration of shallow curved micro/nano-beam based on strain gradient theory under thermal loading with temperature-dependent properties", *Appl. Phys. A*, **123**(1), 4. https://doi.org/10.1007/s00339-016-0591-9.

Shen, H.S. and Zhu, Z. (2012), "Postbuckling of sandwich plates with nanotube-reinforced composite face sheets resting on elastic foundations", *Eur. J. Mech. A Solids*, **35**, 10-21. https://doi.org/10.1016/j.euromechsol.2012.01.005.

Shenas, A.G., Malekzadeh, P. and Ziaee, S. (2017), "Vibration analysis of pre-twisted functionally graded carbon nanotube reinforced composite beams in thermal environment", *Compos. Struct.*, **162**, 325-340. https://doi.org/10.1016/j.compstruct.2016.12.009.

Sherigara, B.S., Kutner, W. and D'Souza, F. (2003), "Electrocatalytic properties and sensor applications of fullerenes and carbon nanotubes", *Electroanalysis*, **15**(9), 753-772. https://doi.org/10.1002/elan.200390094.

Şimşek, M. (2011), "Nonlocal effects in the forced vibration of an elastically connected double-carbon nanotube system under a moving nanoparticle", *Comput. Mater. Sci.*, **50**(7), 2112-2123. https://doi.org/10.1016/j.commatsci.2011.02.017.

Sinha, N. and Yeow, J.W. (2005), "Carbon nanotubes for biomedical applications", *IEEE Trans. Nanobiosci.*, **4**(2), 180-195. https://doi.org/10.1109/TNB.2005.850478.

Suehiro, J., Zhou, G. and Hara, M. (2003), "Fabrication of a

carbon nanotube-based gas sensor using dielectrophoresis and its application for ammonia detection by impedance spectroscopy", *J. Phys. D Appl. Phys.*, **36**(21), 109. https://doi.org/10.1088/0022-3727/36/21/L01.

Thess, A., Lee, R., Nikolaev, P., Dai, H., Petit, P., Robert, J., Xu, C., Lee, Y.H., Kim, S.G. and Rinzler, A.G. (1996), "Crystalline ropes of metallic carbon nanotubes", *Science*, **273**(5274), 483-487. https://doi.org/10.1126/science.273.5274.483.

Wang, C., Lv, R., Kang, F., Gu, J., Gui, X. and Wu, D. (2009), "Synthesis and application of iron-filled carbon nanotubes coated with FeCo alloy nanoparticles", *J. Magn. Magn. Mater.*, **321**(13), 1924-1927. https://doi.org/10.1016/j.jmmm.2008.12.013.

Wang, Q. and Liew, K. (2007), "Application of nonlocal continuum mechanics to static analysis of micro-and nano-structures", *Phys. Lett. A*, **363**(3), 236-242. https://doi.org/10.1016/j.physleta.2006.10.093.

Yumura, M. (2003), "Carbon nanotube industrial applications", *AIST Today*, **10**, 8-9.

Zeighampour, H., Beni, Y.T. and Karimipour, I. (2017a), "Wave propagation in double-walled carbon nanotube conveying fluid considering slip boundary condition and shell model based on nonlocal strain gradient theory", *Microfluid. Nanofluidics*, **21**(5), 85. https://doi.org/10.1007/s10404-017-1918-3.

Zeighampour, H., Beni, Y.T. and Karimipour, I. (2017b), "Material length scale and nonlocal effects on the wave propagation of composite laminated cylindrical micro/nanoshells", *Eur. Phys. J. Plus*, **132**(12), 503. https://doi.org/10.1140/epjp/i2017-11770-7.

CC